

NUMERICAL SIMULATION OF CAVITATING FLOWS IN DIESEL INJECTORS BY A HOMOGENEOUS EQUILIBRIUM MODELING APPROACH

N. Dumont, O. Simonin[†] and C. Habchi

Institut Français du Pétrole, Avenue du Bois-Préau
92852 Rueil-Malmaison, France

[†] Institut de Mécanique des Fluides de Toulouse, Allée du Pr. Soula
31400 Toulouse, France

Abstract

Due to excessive stress in the orifice, cavitation occurs in high-pressure Diesel injectors. As experiments are very hard to manage for injection conditions (small-scaled, high-speed flow), a numerical model seems to be the right tool to get a better understanding of the flow features inside and at the exit of the injector nozzle.

The purpose of this paper is to present a simulation code based on a Homogeneous Equilibrium Model. The validation of the code for typical cavitating flow configuration is presented. Then numerical results of cavitating flows in Diesel injectors are shown. Then we report concluding remarks and objectives.

1 Introduction

The simulation of cavitating flows in high-pressure Diesel injectors has become a very challenging topic in the field of computational fluid dynamics. We will not go back over the fact that cavitation has its own length scale and that experiments have to be done only in real-size injector nozzles (see Arcoumanis *et al.* 1999). As a matter of fact, the flow inside the injector nozzle is high-speed, the orifices are small, the injection duration is very short, the pressure is very high. As a result, experimental investigations on real-size nozzles are rare and numerical modelling is the right tool to get a better understanding of the flow topology in the injector.

A discussion on cavitation modeling in Diesel injectors has been previously made in Dumont *et al.* (2000). Two potential ways of numerical simulation have been identified: the Volume of Fluid method (VOF) and the continuum method. But the one that represents the best compromise for high-pressure common rail injector flow modeling is the continuum model. As a matter of fact, the recent investigations show that this method is widely used to simulate this configuration (see Qin *et al.* 2001, Delannoy and Kueny 1990, Chen and Heister 1995, and Schmidt 1997).

The purpose of this paper is to present a new code, called CavIF (Cavitating Internal Flow), based on the same barotropic equation as the one used in the bidimensional (2D) Cavalry code presented in Schmidt (1997) and the same numerical multibloc architecture as the KIVA-MB code (see Amsden *et al.* 1989, and Habchi and Torres 1992). The model solves tridimensional compressible and viscous Navier-Stokes equations. Fluid is considered as single-phased, whose density varies from liquid density to vapor density according to a barotropic equation of state, based on the expression of the local sound speed depending on the local void fraction. This expression considers the fluid homogeneously mixed on the sub-grid scale, and is called Homogeneous Equilibrium Model (HEM).

The resolution of the Navier-Stokes equations is based on a Quasi-Second Order Upwind (QSOU) scheme for convection, and uses a third-order Runge-Kutta scheme for time advancement. Typical NSCBC formulation (see Thompson 1987, Thompson 1990, Poinot and Lele 1992) has been implemented in order to get non-reflective boundary conditions and to solve strong pressure waves propagation.

At first are presented the characteristics of the code: the barotropic equation of state and the numerical solver. Then the code is validated for a well-known case, the collapse of a cavitating bubble in a “semi-infinite” domain which is compared to the temporal integration of the Rayleigh-Plesset equation. The last part of the paper reports numerical results of 2D and 3D cavitation in a typical Diesel injector geometry.

2 Presentation of the code

2.1 Equations of the model

CavIF solves a compressible and viscous Navier-Stokes system, which consists in the continuity equation:

$$\frac{\partial \rho}{\partial t} + \frac{\partial(\rho u_j)}{\partial x_j} = 0, \quad (1)$$

the momentum equation:

$$\frac{\partial(\rho u_i)}{\partial t} + \frac{\partial(\rho u_i u_j)}{\partial x_j} = -\frac{\partial P}{\partial x_i} + \frac{\partial \tau_{ij}}{\partial x_j}, \quad (2)$$

and the equation of state which is described in section 2.2:

$$P = \mathcal{H}(\rho). \quad (3)$$

The void fraction can be defined as:

$$\alpha = \frac{\rho - \rho_l}{\rho_g - \rho_l}. \quad (4)$$

The two-phase flow pattern is not known *a priori*. But In order to fit the limiting cases where one of the two phases is not present, we consider the dynamic viscosity of the mixture as (see Benkenida 1999 for more details):

$$\mu = \frac{\mu_g \mu_l}{\alpha \mu_l + (1 - \alpha) \mu_g}. \quad (5)$$

As can be seen, the flow is considered as laminar, in spite of the fact that the Reynolds number for typical injection configuration is quite high (about 15,000). Nevertheless, regarding the physical stress the fluid experiences in the very low pressure regions, one can assume that the turbulence does not influence cavitation. This is certainly true near the sharp edge corner, where pressure decreases dramatically. Experimental visualizations show that downstream the sharp edge, the interface is wrinkled, and in the reattachment region, turbulence certainly plays a major role in the breakup and coalescence of the collapsing bubbles. According to Ruiz and He (see Ruiz and He 1999), who have shown that turbulence in cavitating flows cannot be modelled as typical turbulence, further research is needed in order to understand the physical processes governing this phenomenon.

2.2 Equation of state

The two-phase flow is considered as an homogeneous mixture {vapour+liquid}. Its density is defined by an equation of state, which is barotropic. In CavIF is used an equation of state based on the expression of the acoustic speed of the two-phase flow formulated by Wallis (Wallis and Graham 1962):

$$\frac{1}{a^2} = [\alpha \rho_g + (1 - \alpha) \rho_l] \left[\frac{\alpha}{\rho_g a_g^2} + \frac{1 - \alpha}{\rho_l a_l^2} \right]. \quad (6)$$

It can be clearly seen from figure 1 that the sound speed of the homogeneous mixture decreases dramatically as soon as the fluid is not composed of a single phase. This can be explained by the multiple reflexions of the waves between the mixture's components interfaces. As a matter of fact, we can almost

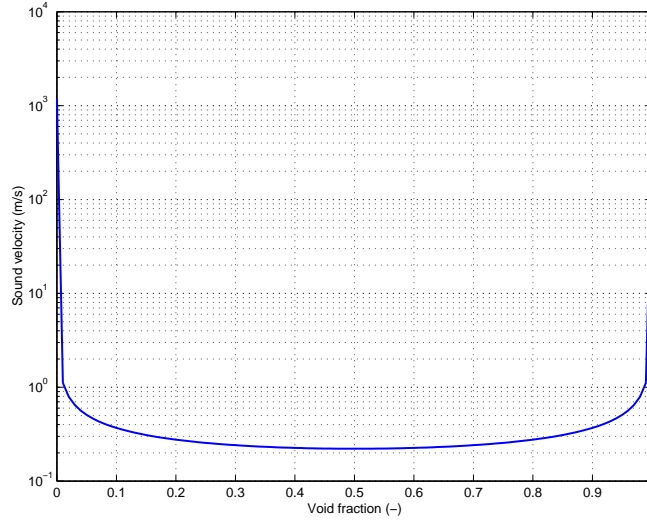


Figure 1: *Sound speed, a , versus void fraction, α .*

consider that, as soon as cavitation appears in a numerical cell, the flow becomes locally supersonic. We will see in sections 2.4.2 and 2.4.4 that this conclusion is very important with regards to boundary conditions.

As we consider the flow as isentropic, we can assume that:

$$a^2 = \frac{dP}{d\rho}. \quad (7)$$

Considering the acoustic speed as constant in pure vapour and pure liquid, we can calculate the equation of state for the two-phase region \mathcal{H} by integrating the expression 7 between the saturation pressure P_l^{sat} and the indicated pressure P (see figure 2):

$$\begin{cases} P = \rho a_g^2 & \text{if } \rho < \rho_g \\ P = P_l^{sat} + \frac{\rho_g a_g^2 \rho_l a_l^2 (\rho_g - \rho_l)}{\rho_g^2 a_g^2 - \rho_l^2 a_l^2} \log \left[\frac{\rho_g a_g^2 (\rho_l + \alpha (\rho_g + \rho_l))}{\rho_l (\rho_g a_g^2 - \rho_l a_l^2)} \right] & \text{if } \rho_g < \rho < \rho_l \\ P = \rho a_l^2 & \text{if } \rho > \rho_l. \end{cases} \quad (8)$$

This equation is used in the code to evaluate analytically P from ρ calculated by the continuity equation.

2.3 Numerical scheme

The numerical scheme for advection consists in a quasi-second order upwind scheme (QSOU) as reported in Amsden *et al.* 1989, which assures the monotonicity of the solution. That is to say that no negative values (by oscillations) can be obtained, despite pressure and density ratios are tremendous. This is very important with regards to calculation robustness. Furthermore, as we have to consider the transient behaviour of cavitation, the time advancement is made thanks to a third-order Runge-Kutta scheme.

The procedure is as follows: $\left(\frac{\partial \rho}{\partial t}\right)^k$ defined at cell centers and $\left(\frac{\partial \rho U}{\partial t}\right)^k$ defined at vertices are calculated from equations 1 and 2 thanks to a finite-volume method. Then, according to Runge-Kutta advancement,

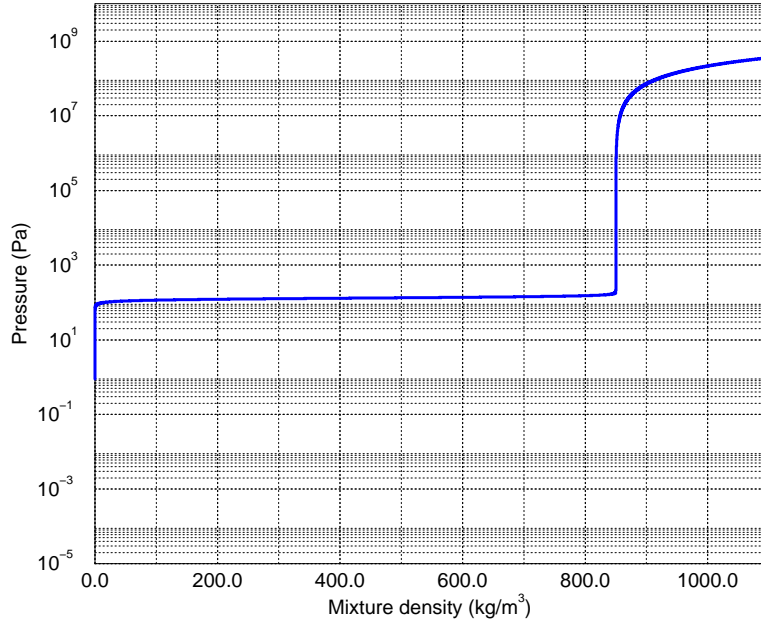


Figure 2: *HEM law of state: $P = \mathcal{H}(\rho)$.*

ρ^k and U^k at pseudo time-step k can be written as, with $k = 1, 2, 3$:

$$\begin{aligned}
 \rho^k &= \gamma^k \left(\frac{\partial \rho}{\partial t} \right)^k \Delta t + \psi^k \left(\frac{\partial \rho}{\partial t} \right)^{k-1} \Delta t + \rho^{k-1} \\
 U^k &= \frac{\gamma^k \left(\frac{\partial \rho U}{\partial t} \right)^k \Delta t + \psi^k \left(\frac{\partial \rho U}{\partial t} \right)^{k-1} \Delta t + \rho_*^{k-1} U^{k-1}}{\rho_*^{k-1}} \\
 P^k &= \mathcal{H}(\rho^k)
 \end{aligned} \tag{9}$$

ρ_*^k is the density calculated at vertices for the pseudo-time step k , γ^k and ψ^k the Runge-Kutta scheme constants.

As we use an explicit scheme the time step has to obey the following stability criterions :

$$\begin{aligned}
 (|U| + a) \frac{\Delta t}{\Delta x} &< 1, \\
 \frac{\mu \Delta t}{\rho \Delta x^2} &< 1.
 \end{aligned} \tag{10}$$

2.4 Boundary conditions

Due to the strongly transient behaviour of the flow and pressure waves propagation, one has to compute boundary conditions which allow control of the different waves that cross the boundaries. Indeed, most of the simulation codes which are used nowadays model the injector exit as an imposed pressure, i.e. chamber pressure (P_{ch}). But as cavitation is closely related to pressure field, numericals results show that no cavitation structures can reach the injector exit. In fact, they “collapse” numerically as soon as they reach the exit boundary.

To prevent from this problem, one has to model more appropriate boundary conditions that can take in account pressure waves propagation. For the inlet, the Bernoulli equation is written between a stagnation point (at conditions P_{inj} , ρ_{inj}) and the inlet cells (at conditions P_{in} , ρ_{in}). The pressure P_{in} is calculated thanks to a finite difference between the stagnation point and the nearest cell pressure P_{near} . β is a relaxation coefficient.

$$P_{in} = P_{inj} + \beta(P_0 - 2P_{in} + P_{near}) \quad (11)$$

The inlet velocity direction is assumed perpendicular to the cell inlet face, and its magnitude U_{in} is:

$$U_{in} = \sqrt{2 \left(\frac{P_{inj}}{\rho_{inj}} - \frac{P_{in}}{\rho_{in}} \right)} \quad (12)$$

Those boundary conditions allow the pressure from the interior of the domain to influence the inlet pressure, as we consider the inlet as subsonic and non cavitating.

On the wall, velocity is set to zero.

At the exit, typical NSCBC (Navier-Stokes Characteristic Boundary Conditions) seem to be the best approach for this type of flow. The method that we use consists in expressing inviscid Navier Stokes equations as characteristic equations at the exit.

The procedure is as follows: \vec{n} is the outward normal vector of each exit boundary cell face, $\vec{\tau}$ and \vec{b} are two vectors which form the local vector base (\vec{n} , $\vec{\tau}$, \vec{b}). Velocities (u_n, u_τ, u_b) are the tridimensional velocities expressed in the local base.

After calculations of characteristic equations, the conservative system at the exit can be written:

$$\begin{aligned} \frac{\partial \rho}{\partial t} + \frac{\rho}{a} (\mathcal{L}_4 - \mathcal{L}_1) &= 0 \\ \frac{\partial \rho u_n}{\partial t} + \frac{u_n \rho}{a} (\mathcal{L}_4 - \mathcal{L}_1) + \rho (\mathcal{L}_1 + \mathcal{L}_4) &= 0 \\ \frac{\partial \rho u_\tau}{\partial t} + \frac{u_\tau \rho}{a} (\mathcal{L}_4 - \mathcal{L}_1) + \rho \mathcal{L}_2 &= 0 \\ \frac{\partial \rho u_b}{\partial t} + \frac{u_b \rho}{a} (\mathcal{L}_4 - \mathcal{L}_1) + \rho \mathcal{L}_3 &= 0, \end{aligned} \quad (13)$$

where the \mathcal{L}_i 's are the characteristic waves amplitudes, and the λ_i 's are the propagation velocities of each characteristic wave, defined as:

$$\begin{aligned} \lambda_1 &= u_n - a \\ \lambda_2 &= \lambda_3 = u_n \\ \lambda_4 &= u_n + a. \end{aligned} \quad (14)$$

For subsonic outward flow, λ_1 and λ_4 represent the velocities of the sound waves moving in the $-\vec{n}$ and \vec{n} directions, respectively. λ_2 and λ_3 are the velocities at which u_τ and u_b are advected by the flow in the \vec{n} direction.

It can be seen that the waves are assumed to travel only in the normal direction. As a matter of fact, this can be regarded as a limitation of the boundary conditions. Nevertheless, building an exit frontier as perpendicular to the flow (and more specifically perpendicular to the wave propagation direction) as possible is quite obvious for CFD calculations.

The wave amplitudes values (\mathcal{L}_i) are defined as:

$$\begin{aligned}
\mathcal{L}_1 &= \frac{1}{2}(u_n - a) \left[-\frac{a}{\rho} \frac{\partial \rho}{\partial n} + \frac{\partial u_n}{\partial n} \right] \\
\mathcal{L}_2 &= u_n \frac{\partial u_\tau}{\partial n} \\
\mathcal{L}_3 &= u_n \frac{\partial u_b}{\partial n} \\
\mathcal{L}_4 &= \frac{1}{2}(u_n + a) \left[\frac{a}{\rho} \frac{\partial \rho}{\partial n} + \frac{\partial u_n}{\partial n} \right].
\end{aligned} \tag{15}$$

Depending on the exit flow configurations, several cases have to be considered.

2.4.1 Subsonic outflow

In that case, all λ_i 's are positive, except for $i = 1$. That means that the \mathcal{L}_i 's can be estimated from the interior values (as waves move outward), thanks to the equations 15, whereas the \mathcal{L}_1 value is obtained by considering the chamber pressure (P_{ch}) as constant. If the outlet pressure is not close to the P_{ch} prescribed value, incoming wave will enter the domain in order to bring the outlet pressure value back to P_{ch} .

\mathcal{L}_1 can be simply expressed by:

$$\mathcal{L}_1 = \kappa(P - P_{ch}), \tag{16}$$

where a mechanical analogy with the spring is obvious. The main point now is to determine κ in order to get the best behaviour as possible at the exit. It can be noted that, by setting $\kappa = 0$, we get the so-called ‘‘perfectly non-reflecting’’ conditions.

2.4.2 Supersonic outflow

As we have seen in section 2.2, sound speed is strongly dependent on void fraction. As cavitation can reach the injector exit, local sound speed can decrease to very low values, leading to local supersonic flow. In that case, all \mathcal{L}_i 's are estimated from the interior of the domain as no wave can enter from the exit. The set of equations 15 is then used to compute \mathcal{L}_i values. This statement is very important: when cavitation reaches the injector exit, no relaxation over the exit pressure P_{ch} is made, and cavitation can normally leave the domain, without any numerical collapse.

2.4.3 Subsonic inflow

The topology of the flow in Diesel injector can lead to ‘‘hydraulic flip’’ (see Yule *et al.* 1998, Tamaki *et al.* 1998, Soteriou *et al.* 1995), as recirculation zones reach the orifice outlet. In that case, the flow enters the domain and the λ_i 's are negative except λ_4 . So \mathcal{L}_4 can be calculated from the interior values (see equation 15), and the other wave amplitudes are given by the following equations:

$$\begin{aligned}
\mathcal{L}_1 &= \kappa(P - P_{ch}), \\
\mathcal{L}_2 &= \mathcal{L}_3 = 0.
\end{aligned} \tag{17}$$

2.4.4 Supersonic inflow

This case hardly happens but to be consistent one has to model this configuration too. For supersonic inflow, all propagation velocities are negative, so all \mathcal{L}_i values need to be modeled from outside of the domain.

$$\begin{aligned}
\mathcal{L}_1 &= \kappa(P - P_{ch}), \\
\mathcal{L}_2 &= \mathcal{L}_3 = 0, \\
\mathcal{L}_4 &= \kappa(P - P_{ch}).
\end{aligned} \tag{18}$$

3 Validation of the cavitation model

3.1 Collapse of a symmetric bubble

In order to validate the numerical scheme and the barotropic equation of state, one has to simulate a well-known test case: the collapse of a symmetric bubble in an infinite domain. The study of the bubble dynamics has been performed by Rayleigh and Plesset, considering that:

- the bubble shape remains spherical,
- the bubble is very small compared to the liquid volume, and that liquid has a newtonian behaviour,
- liquid is incompressible.

That study leads to Rayleigh-Plesset equation:

$$\rho \left[R \frac{d^2 R}{dt^2} + \frac{3}{2} \left(\frac{dR}{dt} \right)^2 \right] + \frac{4\mu}{R} \frac{dR}{dt} = \left(P_{\infty 0} - P_{sat} + \frac{2\sigma}{R_{init}} \right) \left(\frac{R_{init}}{R} \right)^{3k} - P_{\infty} + P_{sat} - \frac{2\sigma}{R}. \quad (19)$$

As CavIF does not handle surface tension effects and incondensable gaz (i.e. the bubble content is pure vapour), this equation simplifies in this way:

$$\rho \left[R \frac{d^2 R}{dt^2} + \frac{3}{2} \left(\frac{dR}{dt} \right)^2 \right] + \frac{4\mu}{R} \frac{dR}{dt} = -P_{\infty} + P_{sat}. \quad (20)$$

The integration is made thanks to a fourth-order Runge-Kutta scheme, and can be compared to the so-called Rayleigh time:

$$T = 0.915 R_{init} \sqrt{\frac{\rho}{P_{\infty} - P_{sat}}} \quad (21)$$

In order to simulate a semi-infinite domain, the computational domain which must be far bigger than the bubble, in order to prevent from wall effects before the end of the collapse. The test is performed on a $50 * 50 * 50$ grid. In figure 3 is showed the comparizon between the numerical and theoretical results of the radius evolution versus time, for a bubble of radius $1mm$. It can be seen that at the beginning of the

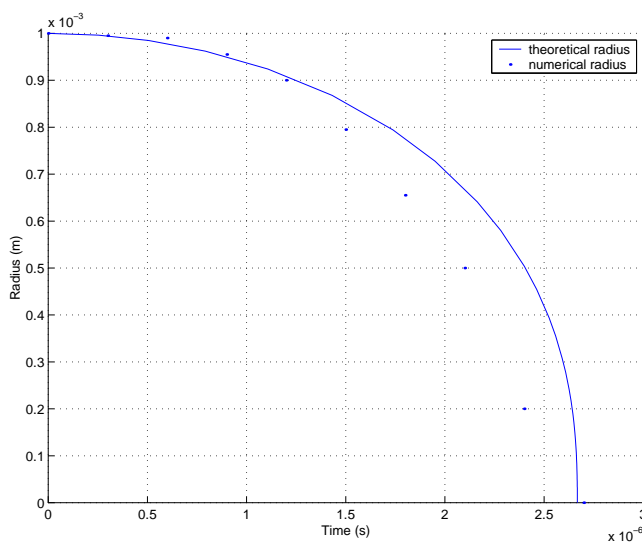


Figure 3: Bubble radius versus time. $R_{init} = 1mm$.

collapse, the model agrees very well with the theoretical results. At the end of the collapse, the bubble resolution becomes so poor that the numerical code cannot take in account the collapse energy. Therefore, the numerical collapse time is about the same than the theoretical one, but the interface is not sufficiently discretized, which results in a bad resolution of the collapse speed. Nevertheless, the agreement is quite good, validating the cavitation and dynamics model.

After the collapse, a pressure wave radiating from the collapse point (where the energy is confined at the end of the collapse) is resolved numerically, as can be seen in collapse visualizations.

3.2 Collapse of an asymmetric bubble

During the collapse of a bubble close to a wall, a jet is formed, which impacts on the rigid boundary. The pressure wave generated by jet impact results in cavitation erosion. The test is performed on a $30 * 30 * 30$ grid. The bubble's center is placed one diameter away from the wall. The inner pressure is seven orders of magnitude lower than the surrounding pressure. We can see in figure 4 the processus of collapse near a

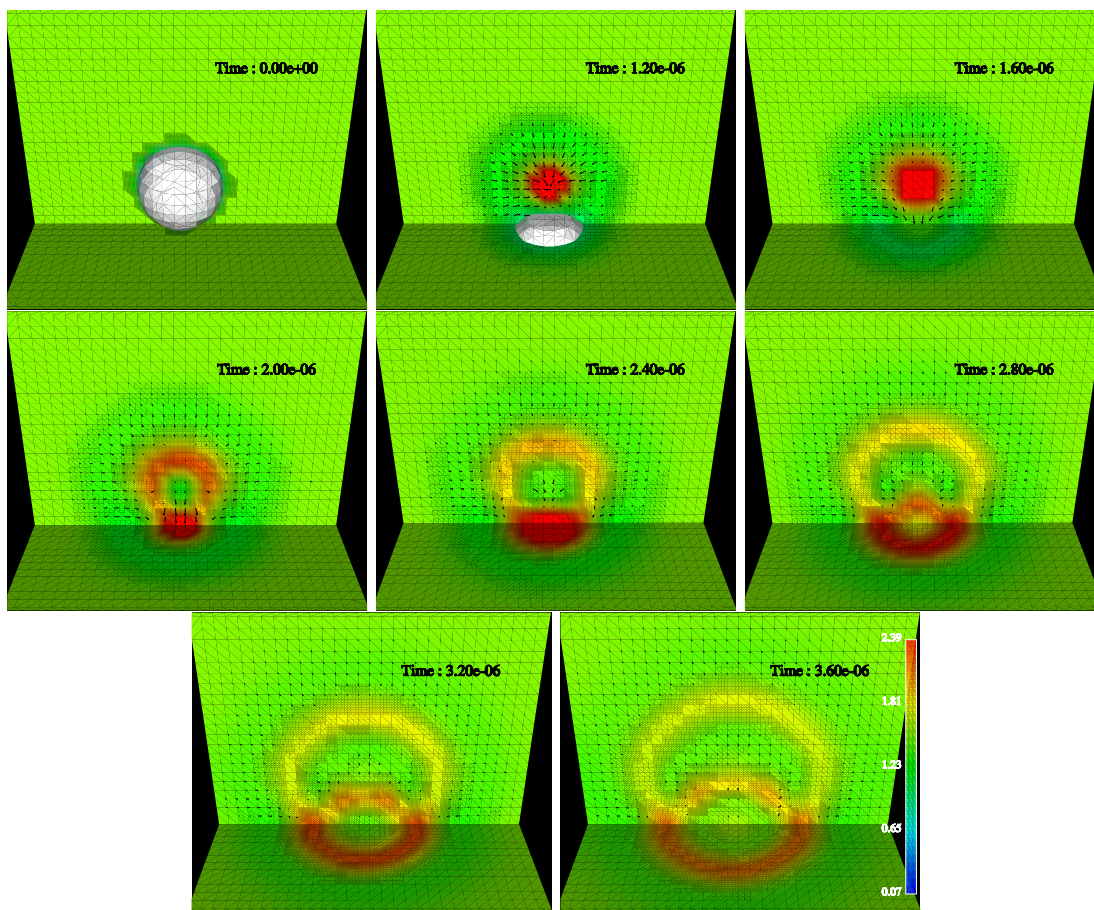


Figure 4: *Collapse of a bubble near a wall. The mixture density is represented, and the isosurface is fixed for $\alpha = 0.9$.*

rigid boundary: at $1.2 * 10^{-6}$ s, the bubble has already collapsed, and a depression region has been formed on the wall surface, which leads to the formation of a liquid jet which is directed towards the boundary (at $1.6 * 10^{-6}$ and $2.0 * 10^{-6}$ s). We can remark the formation of a strong pressure wave radiating from the end-of-collapse zone. As the jet hits the physical boundary, a strong pressure wave (far greater than the first) is formed. Later, we can remark that the second pressure wave results in the combination of two effects

(see at $2.4 * 10^{-6}$ s): the jet hits the wall, and the first pressure wave reaches the wall too, increasing the energy concentration in this region.

The numerical results are in agreement with the qualitative experimental results: it has been seen that during the collapse, a strong pressure wave is formed on the rigid boundary, which leads to damages in typical industrial applications.

4 Results and Discussions

4.1 2D injector

A classical bidimensional geometry is used to simulate the flow in a typical Diesel injector. The main point of this study is to identify the flow topology in a single hole nozzle, for typical injection configuration: $P_{inj} = 1000bar$ and $P_{ch} = 50bar$. The orifice is $1mm$ long, and its diameter is $0.2mm$ ($\frac{L}{D} = 5$).

The initial conditions are as follows: the nozzle is full of liquid fuel at an initial pressure of $50bar$. The inlet total pressure is fixed at $1000bar$. Consequently, a compression wave develops inside the nozzle. As soon as the pressure wave reaches the exit, NSCBC relax the outlet pressure back to $50bar$. Then the fluid is strongly accelerated through the constriction. As we can see in figure 5, a recirculation region is

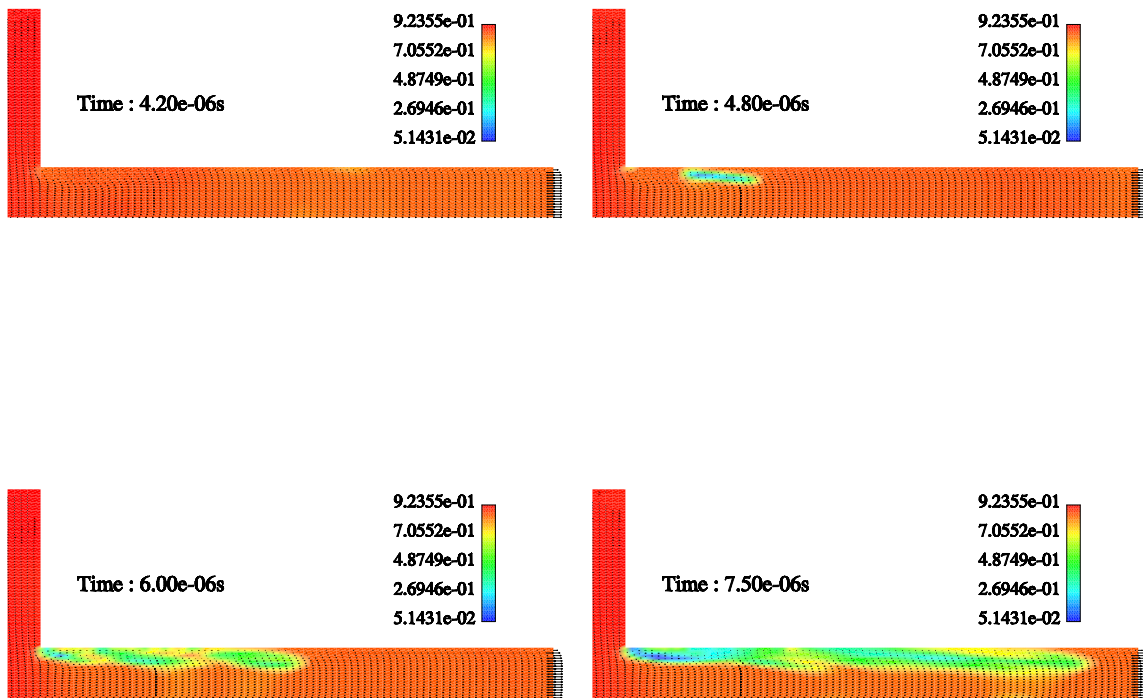


Figure 5: *Apparition of cavitation in a single hole orifice. Mixture density in g/cm^3 .*

formed downstream the sharp edge, which results in cavitation at $4.8 * 10^{-6}$ s. Then this cavitation elongates throughout the orifice and reaches the exit at $t = 8 * 10^{-6}$ s (see figure 6). We can see in figures 7 and 8 the behaviour of the cavitation length. The tremendous pressure drop at the entry corner causes a strong decrease of the mixture density (see figure 8), which then relaxes along the nozzle. The rising of the mixture density downstream of the corner can be explained by the collapse and the breakup of cavitation along the orifice. Nevertheless, the exit density profile (see figure 9) shows that cavitation is still strongly present as the “liquid jet” leaves the injector and enters the combustion chamber.

The topology of the flow is similar to Soteriou visualizations (see Soteriou 1999), showing a large vapour pocket attached to the sharp edge inlet, and the cavitation which is located within the attached boundary layer.

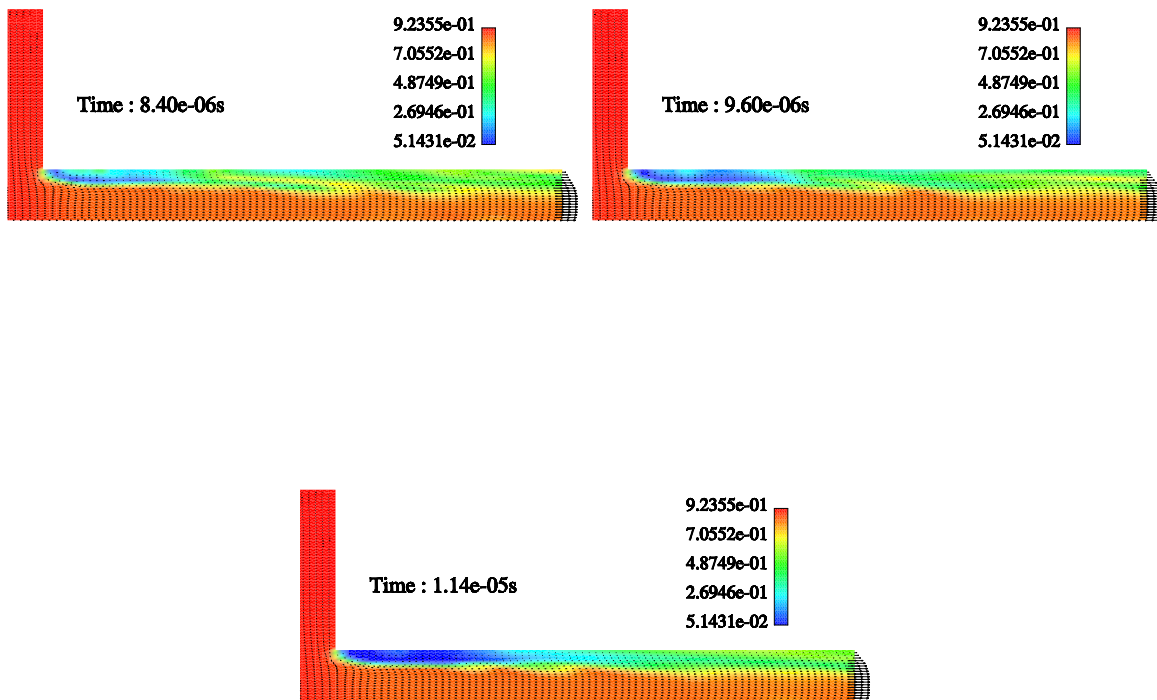


Figure 6: *Stabilization of cavitation in a single hole orifice. Mixture density in g/cm^3 .*

Considering the flowrate exiting from the nozzle, we can remark that, as soon as cavitation reaches the injector exit, the flow behaves as it was “choked” and the discharge coefficient remains constant at $Cd = 0.62$. This result can be compared to Ohrn experimental results (see Ohrn *et al.* 1991). In fact, the flow remains attached until cavitation reaches the exit, as can be seen in figure 5. This can be clearly seen in figure 10, as the discharge coefficient continues to grow until $8 * 10^{-6}$ s. At that time, cavitation reaches the exit and the flow becomes completely detached, leading to a well-known flowrate limitation.

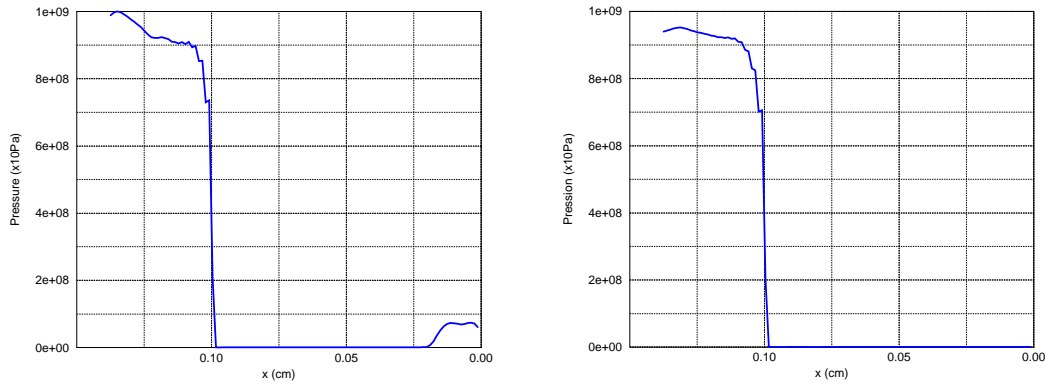


Figure 7: Pressure profiles near the nozzle wall. Left: at $t=7.5 * 10^{-6} s$. Right: at $t=11.4 * 10^{-6} s$.

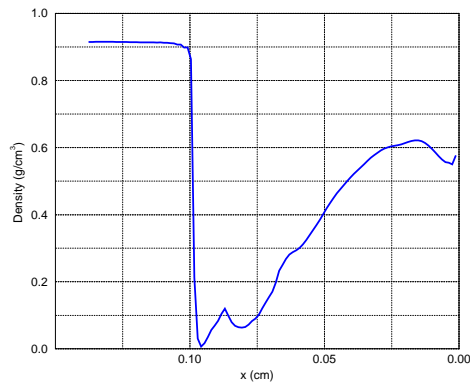


Figure 8: Density profile at $t=11.4 * 10^{-6} s$ near the nozzle wall.

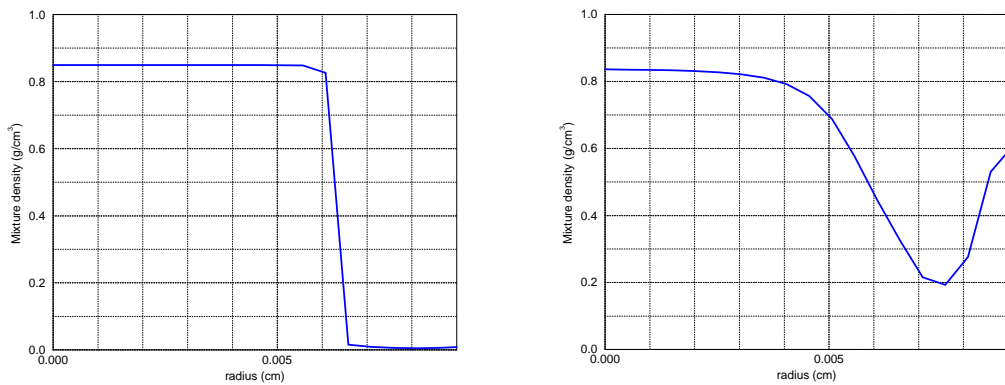


Figure 9: Mixture radius profiles for stabilized flow. Left: immediately downstream the inlet corner. Right: at the exit.

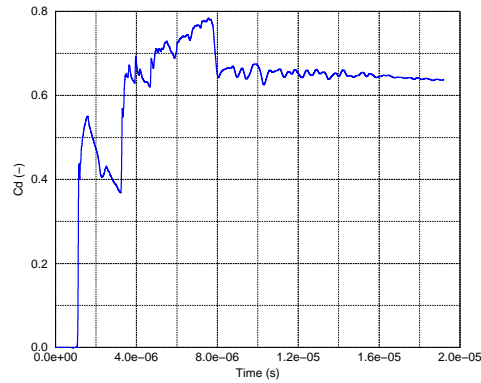


Figure 10: Cd versus time.

These results are in accordance with experimental visualizations and measurements, validating the code for a typical injection configuration.

5 3D results

In order to have a better understanding of the cavitating flow in Diesel injector nozzle, one has to model the flow in the whole geometry as reported in Dumont *et al.* (2000). In this paper are presented 3D results of cavitation in a single hole sharp-edge injector. The geometry is discretized thanks to a cartesian mesh of 160,000 cells, as can be seen in figure 11. The orifice length is $1mm$, its diameter $0.2mm$. The injection conditions are: $P_{inj} = 1000bar$, $P_{ch} = 50bar$.

The numerical results are shown in figure 12. Cavitation develops in the same way as previously seen for the

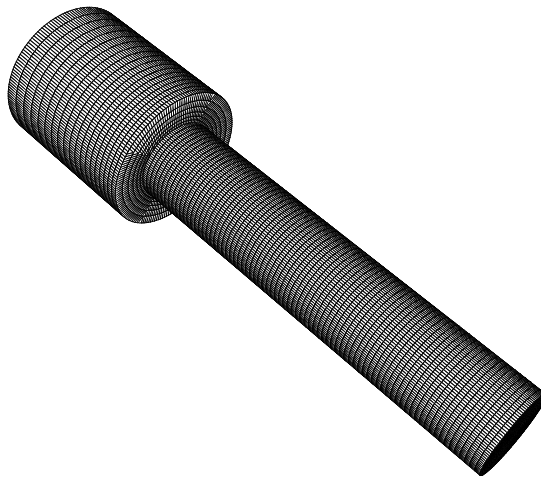


Figure 11: 3D geometry of a single-hole injector.

bidimensional case: There is at first the formation of cavitation in the recirculation region just downstream of the sharp edge corner. Then the cavitation remains attached at the corner, and develops downstream within the boundary layer. As soon as cavitation reaches the exit, the flow becomes choked, and the discharge coefficient stabilizes at 0.62.

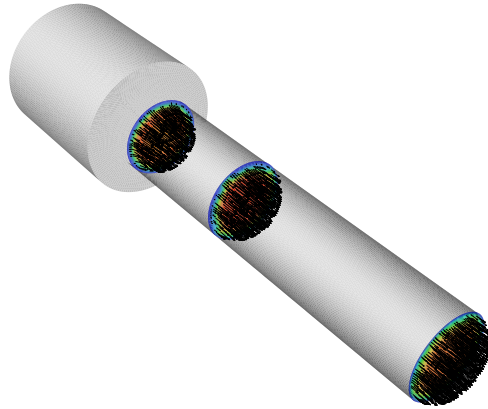


Figure 12: *Density for the 3D case and velocity vectors.*

The 3D results are in accordance with 2D results and experimental data. This is promising for the simulation of an injection in a multi-hole injector.

6 Conclusion

In this paper has been presented a 3D, viscous, unsteady numerical tool which is able to predict cavitation in small orifices, such as Diesel injectors. The code has been validated against bubble collapse modelling, in order to show that a barotropic equation of state for the fluid is suitable for cavitation simulation.

An example of 2D calculations in a typical Diesel injector geometry has been shown. The results indicate that cavitation can get out of the injector and reach the combustion chamber (this has already been shown experimentally). Consequently, we can note that the boundary conditions for this type of code is of primary importance with regards to cavitation modelling.

The computed 3D case has allowed us to validate the code for a single hole configuration. The multi-bloc architecture of the code will make possible calculations in complicated geometries (multi hole injectors), in order to quantify the effects of the injector geometry on the flow topology, especially on the flow behaviour at the injector exit.

Acknowledgements

The authors wish to thank Prof. David P. Schmidt (University of Massachusetts) for his help and collaboration.

References

- Amsden, A., O'Rourke, P., and Butler, T. (1989). Tech. Report No. LA-11560-MS, Los Alamos National Lab.
- Arcoumanis, C., Flora, H., Gavaises, M., Kampanis, N., and Horrocks, R. (1999). *SAE Paper*, 1999-01-0524.
- Benkenida, A. (1999). Ph.D. Thesis, INP Toulouse.
- Chen, A., and Heister, H. (1995). *Comp. Fluids*, **24**, No. 7.

- Delannoy, B., and Kueny, H. (1990). *ASME Cavitation and Multiphase flow forum*, **98**, 153-158.
- Dumont, N., Simonin, O., and Habchi, C. (2000). *International Conference on Liquid Atomizations and Spray Systems 2000 Proceedings*.
- Habchi, C., and Torres, A. (1992). *First European CFD Conference Proceedings*, **1**, 502-512.
- Ohrn, T.R., Senser, D.W., and Lefebvre, A.H. (1991). *Atomization and Sprays*, **1**, No 2, 137-153.
- Poinsot, T., and Lele, S. (1992). *J. Comp. Phys.*, **101**, 104-129.
- Qin, J.-R., Zhang, Z.-C., and Lai, M.-C. (2001). *Eleventh International Multidimensional Engine Modeling User's Group Meeting*.
- Ruiz, F., and He, L. (1999). *Atomization and Sprays*, **9**, 419-429.
- Schmidt, D. (1997). Ph.D. Thesis, University of Wisconsin, Madison.
- Soteriou, C., Andrews, R., and Smith, M. (1995). *SAE Paper*, 950080.
- Soteriou, C., Andrews, R., and Smith, M. (1999). *SAE Paper*, 1999-01-1486.
- Tamaki, N., Shimizu, M., Nishida, K., and Hiroyasu, H. (1998). *Atomization and Sprays*, **8**, 179-197.
- Thompson, K. (1987). *J. Comp. Phys.*, **68**, 1-24.
- Thompson, K. (1990). *J. Comp. Phys.*, **89**, 439-461.
- Wallis, and Graham. (1969). *One-dimensional two-phase flow*, Mc Graw-Hill.
- Yule, A., Dalli, A., and Yeong, K. (1998). *ILASS Europe '98 Proceedings*, 230-235.